Scott Brooks ORCID iD: 0000-0002-8437-9788

Ecosystem controls on methylmercury production by periphyton biofilms in a contaminated stream: Implications for predictive modeling

Grace E. Schwartz[1], Todd A Olsen[2], Katherine A. Muller[3], Scott C. Brooks[1]*

[1]Environmental Sciences Division, Oak Ridge National Laboratory, P.O. Box 2008, MS 6038, Oak Ridge, TN 37831-6038

[2]Present address: Geosyntec Consultants, 3043 Goal Canal Drive, Suite 100, Rancho Cordova, CA, 95670

[3]Present address: Pacific Northwest National Laboratory, PO Box 999, Richland, WA 99352

*Address correspondence to brookssc@ornl.gov

Running head: Controls on methylmercury production by periphyton biofilms

ACKNOWLEDGMENTS

This work was funded by the U.S. Department of Energy, Office of Science, Biological and Environmental Research, Subsurface Biogeochemical Research Program and is a product of the Science Focus Area (SFA) at ORNL. KAM was supported by the U.S. Department of Energy's Oak Ridge Office of Environmental Management (OROEM) and URS | CH2M Oak Ridge LLC (UCOR) as part of ORNL's Mercury Remediation Technology Development Program. The isotopes used in this research were

supplied by the United States Department of Energy Office of Science by the Isotope Program in the Office of Nuclear Physics.

DATA ACCESSIBILITY STATEMENT

Data associated with this manuscript is available in the Supplementary Information file.

ABSTRACT

Periphyton biofilms produce a substantial fraction of the overall monomethylmercury (MMHg) flux in East Fork Poplar Creek, an industrially contaminated, freshwater creek in Oak Ridge, Tennessee (Olsen 2016). We examined periphyton MMHg production across seasons, locations, and light conditions using mercury stable isotopes. Methylation and demethylation rate potentials ($k_{m,\ trans\ av}$, and $k_{d,\ trans\ av}$, respectively) were calculated using a transient availability kinetic model. Light exposure and season were significant predictors of $k_{m,\ trans\ av}$, with greater values in full light exposure and in the Summer. Season, light exposure, and location were significant predictors of $k_{d,\ trans\ av,}$ which was highest in dark conditions, in the Spring, and at the upstream location. Light exposure was the controlling factor for Net MMHg production, with positive production for periphyton grown under full light exposure and net demethylation for periphyton grown in the dark. Ambient MMHg and $k_{m,\ trans\ av}$ were significantly correlated. Transient availability rate potentials were 15× higher for k_m and 9× higher for k_d compared to full availability rate potentials ($k_{m,\ full\ av}$ and $k_{d,\ full\ av}$) calculated at 1d. No significant model for the prediction of $k_{m,\ full\ av}$ or $k_{d,\ full\ av}$ could be constructed using Light, Season, and Location. Additionally, there were no significant differences among treatments for the full availability $k_{m,\ full\ av}$, $k_{d,\ full\ av}$, or Net MMHg calculated

using the full availability rate potentials. $k_{m,\,full\,av}$ was not correlated with ambient MMHg concentrations. Our results underscore the importance of applying transient availability kinetics to MMHg production data when estimating MMHg production potential and flux.

Graphical Abstract

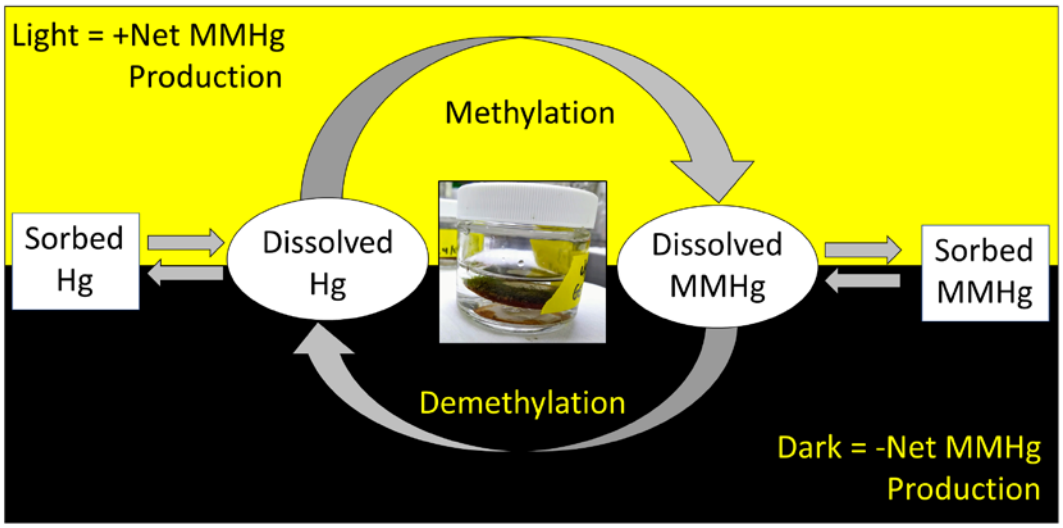

Keywords: periphyton, methylmercury, kinetics

INTRODUCTION

The conversion of mercury (Hg) to monomethylmercury (MMHg) is a key area of concern in global Hg cycling. MMHg is a potent neurotoxin (Clarkson 2003) that biomagnifies in aquatic species and presents a human health risk, particularly for developing fetuses and young children. The conversion of Hg to MMHg is mediated by anaerobic microorganisms (Gilmour 2013) and occurs in a number of diverse habitats (Podar 2015), including periphyton biofilms (Dranguet 2017a).

Periphyton biofilms comprise complex consortia of microorganisms including algae, fungi, *Bacteria,* and *Archeae* that are attached to inorganic and organic substrates in aquatic environments (Battin 2016). These biofilms can contain steep gradients of oxygen on the microscopic scale (Jørgensen 1979; Revsbech 1983), and MMHg is generated by sulfate-reducing, iron-reducing, and methanogenic bacteria that occupy the anoxic niches within the biofilm (Achá 2011; Achá 2012; Gentès 2017; Hamelin 2011).

MMHg production by biofilms is highly variable and depends on a variety of environmental factors including, temperature, light, and dissolved oxygen (Dranguet 2017a). These factors can impact MMHg production directly by shaping the microbial community (Christensen 2018; Graham 2018), or indirectly by affecting algal growth, biomass, and metabolites exuded. There is little evidence that periphyton algae directly methylate mercury (Grégoire and Poulain 2014), however, algae can support MMHg production indirectly by providing structure to biofilms that harbor methylating bacteria (Olsen 2016), exuding metabolites that stimulate Hg-methylating microorganisms, and by releasing chemicals that enhance Hg uptake into methylating bacteria. For example, algae secrete labile organic carbon, which can stimulate Hg-methylating bacteria (Bravo 2017; Kucharzyk 2015) and may also increase Hg uptake by methylating bacteria (Graham 2012; 2013; Mangal 2019b), though this appears to depend on the character of the algal organic carbon (Mangal 2019b). Algae also exude low molecular weight (LMW) thiols (Leclerc 2015), which can enhance Hg bioavailability to bacterial cells (Schaefer and Morel 2009; Schaefer 2011).

Maximum periphyton MMHg production occurs in warmer temperatures (20 to 25°C) (Desrosiers 2006; Olsen 2016), as low temperatures reduce microbial activity. Reports on the impact of light on MMHg production are mixed, with one study showing enhanced periphyton MMHg production in the light (Olsen 2016), while others report higher periphyton MMHg production in the dark (Cleckner 1999; Mauro 2002). In light conditions, photosynthesizing algae generate oxygen, which could induce unfavorable conditions for Hg-methylating bacteria. However, full light exposure also enhances biofilm growth, which provides more anaerobic niches for Hg-methylators and increases the amount of algal metabolites exuded, possibly stimulating microbial activity and enhancing Hg uptake.

Previous work in East Fork Poplar Creek (EFPC) in Oak Ridge, Tennessee, USA determined that actively photosynthesizing biofilms in the creek contain zones of MMHg production (Olsen 2016). This study found that the three-dimensional structure of the algal biofilm was important for MMHg production, and higher MMHg production was observed in light-incubated periphyton versus dark treatments. Inter-site differences in net MMHg production in EFPC were driven by differences in the demethylation potential whereas intra-site variability in net MMHg production was driven by temperature dependent methylation potentials, indicating that season might be a significant factor. However, the estimates for MMHg production from the Olsen et al. 2016 study were generated with single-timepoint first-order kinetic models that assumed full-bioavailability of Hg and MMHg. Recently, a new model for MMHg production kinetics has been developed, which accounts for the transient availability of Hg and MMHg for methylation and

degradation reactions over time (Olsen 2018). The transient availability kinetic model provided estimates for periphyton MMHg generation and degradation rate potentials that were 25 times and 5 times higher, respectively, than full availability, single time point estimates (Olsen 2018). It is unknown whether previously observed correlations between MMHg production and temperature, light exposure, and location in EFPC hold when methylation and demethylation rate potentials are calculated from time series data using transient availability kinetics.

In this study, we used EFPC in Oak Ridge, TN as a study site to grow periphyton biofilms *in-situ* at two locations and under two light conditions. The periphyton was harvested over four seasons, and stable Hg isotopes were used to measure methylation and demethylation rate potentials. Our specific objectives were to: (1) Determine the impact of periphyton *in-situ* growth conditions on Hg methylation and MMHg demethylation rate potentials including: location, season, and light exposure; (2) Build a predictive model of net MMHg production in EFPC using growth conditions as factors, and (3) Compare rate potentials generated via the transient availability model to single-time point, full-availability rate potentials.

MATERIALS AND METHODS

Site description. Periphyton was grown on substrates at two sites in EFPC separated by approximately 17 creek kilometers (Upstream site, EFK 5: 36.00175°N, 84.24929°W and Downstream site, EFK 22.3: 35.9662°N, 84.35817°W). A detailed history and characterization of the study sites in EFPC has previously been published (Brooks and Southworth 2011; Olsen 2016; Riscassi 2016). Basic water

quality at both sites was measured when the periphyton was collected for each experiment (Table 1). Surface water chemistry was similar between Upstream and Downstream sites across seasons, with the major difference being Hg (measured as total Hg) and MMHg concentrations.

Study design and biofilm colonization. The impact of *in situ* growth conditions on Hg methylation and MMHg demethylation were examined, including: location (Upstream vs Downstream); season (Winter, Spring, Summer, Fall); and light exposure (direct light, "Light" versus covered, "Dark"). The periphyton biofilms were grown on fritted glass discs (ROBU 30 mm diameter with 10.5 mm hole and 3.5 mm depth) that were attached to submerged structures, which were secured to the creek bed (Figure S1). Previous results demonstrated that biofilms grown on these discs had similar methylation and demethylation activity to those grown on natural creek substrate (Olsen 2016). At each location, half the discs had full light exposure while the other half were covered with black plastic sheeting to block exposure to direct light during growth (Figure S1a). The structures were placed in EFPC at least two months prior to sampling to allow for adequate periphyton growth. Discs were collected from the creek and carried back to the lab for the methylation/demethylation assays and ancillary measurements. Care was taken to avoid disruption of the periphyton structure during disc collection. Four experiments were conducted: Winter (01/29/16), Spring (05/06/16), Summer (08/23/16), and Fall (11/28/16).

Methylation/demethylation assays. Periphyton discs were retrieved from EFPC and placed in 60 mL, clear glass jars with PTFE lined caps for incubations. EFPC surface water (20 mL), collected at the same time as the periphyton discs, was added to each jar. The incubation jars were immediately brought back to the lab to perform the methylation/demethylation assays. At the lab, enriched stable isotopes were spiked into each jar to distinguish new methylation and demethylation activity during the incubations from ambient background MMHg. The enriched, stable isotopes were spiked in the forms of $^{201}HgCl_2$ (methylation monitored by the appearance of $MM^{201}Hg$), and $MM^{202}HgCl$ (demethylation monitored by the loss of $MM^{202}Hg$). The isotopes were purchased from Oak Ridge National Laboratory and were enriched as follows: ^{201}Hg (0.07% 198, 0.13% 199, 0.9% 200, 96.17% 201, 2.62% 202, 0.11% 204) and ^{202}Hg (0.13% 198, 1.41% 199, 0.93% 200, 0.68% 201, 95.86% 202, 0.95% 204). $MM^{202}Hg$ was synthesized in-house using the methylcobalamin method (Bancon-Montigny 2004). A few days prior to the start of each experiment several discs were collected and analyzed for total Hg. Isotope spike amounts were selected to be approximately 20% of the ambient Hg and 100% of the ambient MMHg concentration in the periphyton, based on our record of previously measured MMHg:Hg ratio in EFPC periphyton (Olsen 2016). However actual ambient Hg and MMHg varied with differing biomass growth between seasons and light treatments, and the isotope spikes ranged between 20-2500% of the ambient measured Hg and MMHg in the periphyton (Table S1).

An environmental chamber (Conviron CMP 3244) was used to control assay temperatures (20 °C for Spring, Summer, and Fall samples and at 10 °C for Winter

samples). The environmental chamber temperatures were chosen to reflect the average water temperature that the periphyton was exposed to during the several weeks prior to harvest. The chamber light source was kept on for the entirety of each assay. The light level averaged 600 Lux total light intensity (HOBO Pendant Temperature/Light Data Logger, UA-002-64). Dark treatments were wrapped in aluminum foil to prevent light exposure during the incubation. Though light/dark cycles and tree canopy cover change with season in EFPC, constant light and dark conditions were chosen for the incubations to clearly delineate light and dark effects.

The methylation/demethylation incubations were conducted over the course of 3 days (Winter) and 1 day (Spring, Summer, Fall). Each assay had a total of four timepoints, with triplicate jars sacrificed at each timepoint. Winter timepoints were at 6h, 24h, 48h, and 72h. Spring, Summer, and Fall timepoints were at 9min, 3h, 11h, and 24h. At every time point, the incubation jars were frozen (-20 °C) until processing for MMHg analysis. Creek water and killed periphyton controls were analyzed with each experiment. Killed periphyton controls were autoclaved (30 min at 120 °C and 158.6 kPa) before adding stable Hg isotope tracers. Control results are summarized in the SI (Tables S2 and S3).

Analytical methods. For ambient Hg analysis, periphyton samples were digested in aqua regia (0.1 g-dry weight (dw) into 4 mL) followed by dilution with Milli-Q water, $SnCl_2$ reduction and then analysis on the Brooks Rand MERX Total-Hg Purge & Trap Model III AFS with isotope dilution (US EPA 2001b). For MMHg

analysis, periphyton samples were extracted following a previously published method (Bloom 1997). Briefly this method consisted of an acid digestion-methylene chloride extraction followed by a back extraction into water. The extracted samples were then distilled following EPA Method 1631 to further reduce the amount of ambient inorganic Hg in the samples (US EPA 2001a). After distillation, the sample was ethylated and MMHg was measured using a Brooks Rand MERX Hg Speciation GC & Pyrolysis coupled to an ELAN DRC-e ICP-MS with isotope dilution (Meija 2006; US EPA 2001a). Quality assurance/Quality control parameters are summarized in Table S4.

For each experiment, six of the periphyton discs from both the Light and the Dark treatments were freeze-dried to determine the average wet/dry ratio of the periphyton. Microelectrode voltammetry was used to obtain a redox profile of the periphyton for the Spring experiment. Details on the method are provided in the SI. Chlorophyll concentration was measured in single replicates of each treatment in each experiment. The chlorophyll was extracted from the periphyton with a 90% (v/v) acetone solution following EPA method 445 (Arar 1997). Chlorophyll was quantified with a Turner Designs 10-AU Fluorometer. Details on the analysis are in the SI section. LMW thiols in the periphyton were measured on single replicates of the Light treatment samples of each experiment. The samples were prepared using previously described methods (Leclerc 2015) and (Zhang 2004) and were measured via high pressure liquid chromatography (HPLC) with fluorescence detection. Details of the analyses are listed in the SI section.

Modeling Methylation and Demethylation Rates. Methylation and demethylation rate potentials were calculated using the transient availability kinetic model previously described by Olsen et al. (2018). The transient availability model incorporates kinetic expressions for multisite sorption of Hg and MMHg and Hg reduction to Hg^0 with methylation/demethylation kinetics to account for these competing processes when estimating methylation/demethylation potentials (Olsen 2018). Transient availability kinetics are described by equations 1 and 2:

$$\frac{d[Hg]}{dt} = -k_m[Hg] + k_d[MMHg] - k_1[Hg] + k_2[Hg_f] - k_3[Hg] + k_4[Hg_s] - k_5[Hg] + k_6[Hg^0] \quad (1)$$

$$\frac{d[MMHg]}{dt} = k_m[Hg] - k_d[MMHg] - k_7[MMHg] + k_8[MMHg_f] - k_9[MMHg] + k_{10}[MMHg_s] \quad (2)$$

where k_m is the methylation rate constant , k_d is the demethylation rate constant, k_1 is the Hg fast site sorption rate constant, k_2 is the Hg fast site desorption rate constant, k_3 is the Hg slow site adsorption rate constant, k_4 is the Hg slow site desorption rate constant, k_5 is the rate constant for the conversion of Hg to Hg^0, k_6 is the rate constant for the conversion of Hg^0 to Hg, Hg_f is the amount of Hg sorbed to fast sorption sites, Hg_s is the amount of Hg sorbed to slow sorption sites, k_7 is the MMHg fast site adsorption rate constant, k_8 is the MMHg fast desorption rate constant, k_9 is the MMHg slow adsorption rate constant, k_{10} is the MMHg slow desorption rate constant, $MMHg_f$ is the amount of MMHg sorbed to fast sites, and $MMHg_s$ is the amount of MMHg sorbed to slow sites.

The first-order system of differential expressions, with temporally variant Hg and MMHg availability, were modeled using an ordinary differential equation solver (ode45) in MATLAB R2016a (The MathWorks, Natick, MA). The transient availability model was fit to the $MM^{201}Hg$ and $MM^{202}Hg$ datasets by adjusting the values of k_m and k_d using a nonlinear fitting routine (nlinfit). Fits were weighted by the standard deviation of each dataset. Rate coefficients for the other kinetic reactions in the model were taken from Olsen et al. (2018) (Olsen 2018). All $k_{m,\ trans\ av}$ and $k_{d,\ trans\ av}$ are listed in SI Table S5.

Single timepoint, first-order methylation and demethylation rate constants ($k_{m,\ full\ av}$ and $k_{d,\ full\ av}$) were calculated with the following equations:

$$k_m = \frac{-\ln\left(1-\frac{[MM^{201}Hg]_t}{[^{201}Hg]_0}\right)}{t} \qquad (3)$$

$$k_d = -ln\left(\frac{[MM^{202}Hg]_t}{[MM202Hg]_0}\right)/t \qquad (4)$$

where $[^{201}Hg]_0$ and $[MM^{202}Hg]_0$ are the initial concentrations of isotopes added to the samples (measured from a spiked Milli-Q water); t is 1d; and $[MM^{201}Hg]_t$ and $[MM^{202}Hg]_t$ are the concentration of those species measured at time 1d. One day was chosen as the timepoint for ease in comparison across seasons. A summary of the methylation and demethylation results can be found in Table S5.

Net MMHg production by periphyton was calculated as follows:

$$Net\ MMHg\ production =$$

$$\left(k_m \times [ambient\ Hg]_{periphyton}\right) - \left(k_d \times [ambient\ MMHg]_{periphyton}\right) \quad (5)$$

where k_m and k_d are the calculated methylation and demethylation rates from the tracer isotope assays determined from either the transient availability model or the single time point method, and [ambient Hg]$_{periphyton}$ and [ambient MMHg]$_{periphyton}$ are the measured concentrations of ambient Hg and MMHg on the periphyton discs.

Statistical Analyses. Statistical analyses were performed in JMP™ (SAS Institute 2018). All data were assessed for normality prior to analysis. Normality was determined via visual assessment and using the Shapiro Wilk test (α=0.05). When necessary, data were transformed for analysis using the natural logarithm. Standard least squares linear models were constructed to determine the significance of Season, Light, and Location for predicting methylation and demethylation rate potentials. Significance was determined with α = 0.05. Significant effects were retained in the final model, and each model was assessed for possible interaction terms among the predictors. Significant differences among treatments were determined by least squared means analysis followed by Tukey's Honest Significant Difference (HSD) test or the student t-test with α=0.05.

RESULTS AND DISCUSSION

Ambient Hg and MMHg in periphyton

The ambient Hg concentrations in the periphyton (Figure 1a) were approximately 2.5-3.5x higher than previously reported sediment Hg concentrations

at the Upstream and Downstream locations (Brooks 2017), while ambient MMHg concentrations (Figure 1b) in the periphyton were comparable with concentrations previously reported in EFPC sediment (0.5-8.5 ng/g-dw). Both periphyton ambient Hg and MMHg concentrations were within the range of concentrations reported at other contaminated sites (Huguet 2010; Žižek 2007). MMHg as a percentage of total Hg was low (<0.1%) (Figure 1c) in all the treatments which is typical of Hg-contaminated sites (Gilmour 2018). Ambient Hg concentrations were significantly higher in the Light samples (37-55 μg/g-dw) compared to the Dark samples (3-7 μg/g-dw) ($p<0.001$, Table S6). There was no statistically significant difference in Ambient Hg among seasons ($p = 0.43$) or location ($p = 0.39$). Ambient MMHg concentrations were also significantly elevated in the periphyton Light treatments (1.3-8 ng/g-dw) compared to the Dark treatments (0.5-3.5 ng/g-dw) across locations and seasons ($p = 0.01$) (Figure 1b, Table S6). There was no significant difference between location ($p= 0.29$) or among season ($p = 0.13$) for ambient MMHg.

It is unclear why the Light periphyton samples contained much higher ambient Hg concentrations than Dark samples on a per gram dry weight basis. Photosynthetic bacteria that are exposed to light can act as a sponge for Hg(II), and photosynthetic biofilms have been shown to increase Hg(II) binding capacity 5 fold (Kis 2017). A characterization of the microbial composition of our biofilms and direct uptake experiments are needed to determine if this is a possible mechanism for Hg accumulation in our Light samples. The simplest explanation for the

phenomenon is that Light samples had more algal biofilm growth and therefore had greater surface area available for Hg sorption.

We observed greater ambient MMHg concentrations in Light samples compared to Dark, which could be due to higher levels of ambient Hg available for methylation, larger biomass that created better anoxic conditions for methylation, or an increase in algal metabolites that stimulated Hg-methylators. Clear oxygen gradients were seen in all the samples tested, and measurements revealed anoxic areas in Light samples from both the Upstream and Downstream sites, confirming that the heavy biofilm growth contained anoxic niches (Figure S2). Oxygen depletion was not observed for the Dark samples from either location, consistent with the sparser biofilm growth. Chlorophyll concentrations were 84 ± 1.6 times higher in the Light treatments compared to the Dark samples across all seasons and locations (Figure S3). These results suggest that the Light treatment periphyton had more active photosynthesis occurring, which may have resulted a greater release of algal metabolites that could stimulate methylation.

While there were significant differences in LMW thiol concentration between locations (Figure S4, discussion in SI), no consistent trend was seen between LMW thiol concentration in Light samples and ambient Hg or MMHg concentration.

Methylmercury Production

Mercury methylation (measured by the appearance of $Me^{201}Hg$) and MMHg demethylation (measured by the loss of $MM^{202}Hg$) occurred in all the periphyton

samples (Figures S5-S8). Minimal methylation and demethylation occurred in the killed periphyton and creek water controls (Tables S2 and S3). This confirms our previous results that live periphyton was required for Hg methylation and MMHg demethylation and that the light source in the environmental chambers did not cause photodemethylation (Olsen 2016).

We applied the transient availability kinetic rate model to calculate methylation and demethylation rate potentials in the periphyton samples. On average, methylation rate potentials ($k_{m,\ trans\ av}$) were 1.8 ± 0.4 times higher in the Light treatments compared to the Dark treatments (Figure 2a). The highest $k_{m,\ trans\ av}$ occurred in the summer months when temperatures were highest and when microbial activity would be expected to be highest. To determine the statistically significant drivers of $k_{m,\ trans\ av}$, we constructed a general linear model with Season, Location, and Light as treatment effects (Figure 2b). Season (p=0.001) and Light (p=0.001) were significant predictors of methylation rate potential ($R^2 = 0.84$, $p < 0.001$; Table S6) with $k_{m,\ trans\ av}$ significantly higher in the Light samples and in the Summer compared to the other seasons. Location had no significant effect (p =0.20) when Light and Season were held constant. Ambient MMHg concentrations were also significantly correlated to methylation rate potentials ($R^2 = 0.63$, $p < 0.001$; Figure S9a, Table S6), indicating that $k_{m,\ trans\ av}$ was a reasonable predictor of ambient MMHg production in EFPC periphyton.

An interaction effect was observed between season and light for the methylation rate potential predictive model (Figure S11). In the field, light and

season covary as day length, light intensity, and tree canopy coverage change with season, in addition to seasonal temperature changes. Adding an interaction term for light and season improved our predictive model (Table S6), changing the significance of Location from not significant (p = 0.2) to significant (p = 0.003). Nevertheless, the model including the light × season interaction effect was not selected to describe the data because inclusion of this effect increased the corrected Akaike Information Criterion (AICc), which is a measure of model quality that balances the goodness of fit of the model and the simplicity of the model. The AICc increased from -199.6 to -185.1 for $k_{m,\ trans\ av.}$

On average, demethylation rate potentials ($k_{d,\ trans\ av}$) were 5.4 ± 0.9 times higher in the Dark samples versus the Light samples across season and location (Figure 3a). Demethylation was significantly higher in the Spring compared to the Fall (p= 0.04) and Winter (0.04). The Upstream site had significantly higher $k_{d,\ trans\ av}$ (p = 0.04) than the downstream site across Light and Season. Light (p < 0.0001), Season (p = 0.006), and Location (p = 0.02) were significant factors in predicting the value of demethylation rate potential (Figure 3b; R^2 = 0.88, p<0.001; Table S6). Similar to the predictive model for $k_{m,\ trans\ av}$, an interaction effect was observed between season and light for the demethylation rate potential predictive model (Figure S11). However, the AICc increased from 42.8 to 68.3 for $k_{d,\ trans\ av}$, and we chose not to include the interaction term in the final model to preserve model quality. There was no correlation between ambient Hg concentrations and demethylation rate potential in the periphyton (R^2 = 0.16, p = 0.13), reflecting that the amount of Hg taken up from the creek is far greater than that produced from

MMHg demethylation. Nor was there a significant relationship between ambient MMHg and $k_{d,\,trans\,av}$ (R^2 = 0.19, p =0.11), indicating overall ambient MMHg concentrations were not dominantly controlled by demethylation.

Net methylation (calculated with equation 3) was significantly impacted by light exposure (p <0.0001), with positive net MMHg production in Light samples and negative net MMHg production in Dark samples (Figure 4, Table S6). Past studies, conducted on periphyton from the Florida Everglades (Cleckner 1999) and lakes in Brazil and Wisconsin (Mauro 2002), have reported greater production of MMHg by periphyton in dark conditions. The researchers hypothesized that photosynthesis declined in the dark, resulting in less oxygen production and a greater prevalence of the anaerobic conditions needed for methylation. Demethylation was not measured in these studies, so it is unclear how demethylation might contribute to overall net methylation.

There are several explanations for the greater net MMHg production in our Light samples. The Light samples grew substantially more biomass than the Dark samples, resulting in a thicker algal mat on the substrate. This thicker mat created more micro-environments conducive to anaerobic conditions, which may have enhanced methylation, regardless of greater oxygen production from photosynthesis. Previous work has demonstrated the importance of three-dimensional structure in MMHg production (Olsen 2016). Active algae would also supply labile organic carbon and other metabolites to the rest of the microbial community, possibly enhancing the activity of Hg-methylators (Bravo 2017). Light

exposure impacted the diversity of algae growing on the periphyton discs with consistently greater algal species diversity in the periphyton grown in the light versus the dark (Table S7 and S8). The microbial population was also likely different between the Light and Dark treatments, resulting in differences in Hg uptake (Dranguet 2017b) and the abundance and activity of mercury methylators and demethylators. We are not aware of any studies examining the Hg methylator community in periphyton grown under differing light conditions, but there is evidence of significant differences in the 16S rRNA profiles of light-grown periphyton compared to shade-grown periphyton (Lehmann 2015). Light exposure has been shown to affect biofilm function in cycling nutrients such as nitrogen (Zhao 2018). A recent study by Mangal et al. (2019) found that for three freshwater algal species, dissolved organic matter exudate chemical structure and its Hg binding characteristics varied with light exposure (Mangal 2019a), which would likely impact Hg bioavailability to methylating microorganisms. Also, just as algae may produce metabolites that enhance methylation, it is possible that, under Dark conditions, algae could release metabolites that enhance demethylation. To our knowledge, the effect of algal exudate on demethylation has not been studied. A more detailed microbial and geochemical characterization of EFPC periphyton biofilms grown under differing light conditions is needed to determine the underlying cause of Light and Dark differences in methylation and demethylation rates. There was no demethylation in the Creek Water controls (Table S3), indicating that photodemethylation did not occur during our experiments. However, photodemethylation is wavelength specific (Black 2012) and is likely greater under

natural light than under the artificial light of the growth chambers. Nevertheless, our data show a clear pattern of greater methylation in the light, which agrees with diurnal patterns in MMHg concentration in EFPC surface water (Brooks 2018).

There were no significant differences in Net methylation among seasons ($p = 0.07$), or the two locations ($p = 0.82$). These results differ from the previous EFPC study which found inter-site differences in net MMHg production driven by differences in k_d and intra-site differences in net MMHg production driven by temperature dependent k_m. However, the methylation and demethylation rate potentials calculated in the 2016 study were based on single-time point assays and first-order kinetic equations that assume full availability of Hg and MMHg (equations 3 and 4).

Single timepoint rates versus Transient availability model rates. We re-calculated our methylation and demethylation rate potentials using the full availability, first order kinetics rate model at 1d ($k_{m,\ full\ av}$, $k_{d,\ full\ av}$) to determine if the overall trends in MMHg production change depending on the method used to calculate the rate potentials (Figure S12). $k_{m,\ trans\ av}$ and $k_{d,\ trans\ av}$ were an average of 15 times higher and 9 times higher than $k_{m,\ full\ av}$ and $k_{d,\ full\ av}$ (Figure 5), respectively. For demethylation, the ratio of transient availability rate potentials to single time point rate potentials was stable across season and location (Figure 5b). The ratio for methylation was more variable, ranging from 10-20 (Figure 5a). The overall trends of $k_{m,\ full\ av}$ and $k_{d,\ full\ av}$ were broadly similar those from the transient availability model. For example, $k_{m,\ full\ av}$ was higher in the Light and in warmer Seasons and $k_{d,}$

$_{full\ av}$ was greater for Dark conditions. However, for $k_{m,\ full\ av}$ and $k_{d,\ full\ av}$, we were unable to construct a significant predictive model using Season, Location, and Light as factors for either methylation or demethylation. Analysis of means using the student t-test or Tukey HSD showed no statistically significant differences among treatments for the $k_{m,\ full\ av}$, $k_{d,\ full\ av}$, and net MMHg calculated with the full availability rate potentials. There was also no strong correlation between $k_{m,\ full\ av}$ and ambient MMHg concentrations ($R^2 = 0.02$, $p = 0.62$), reflecting that, for this data set, rate potentials calculated at 1d, assuming full availability of Hg and MMHg, are not good predictors of overall MMHg production in the periphyton (Figure S9b).

Environmental Implications

Light exposure was consistently the strongest determinant of net methylation in EFPC periphyton. Further exploration of the interplay between Light/Dark growth conditions and periphyton microbial community structure and function are needed to explain differences in MMHg production. However, our observation of light as the driving factor of MMHg production in EFPC periphyton matches well with diel observations of MMHg concentration in surface water in EFPC (Brooks 2018). In surface water, MMHg concentrations peak during the day and reach a minimum at night. Field data also confirms that Season is an important factor governing MMHg production. Between 2012 and 2016, higher surface water MMHg concentrations have been observed in the Spring, Summer, and Fall compared to the Winter at the Upstream and Downstream sites (Figure S13). In EFPC, MMHg is produced both in periphyton biofilms and in creek sediment. In this

study, MMHg production was net negative in periphyton grown in Dark conditions. If the dark hyporheic sediments are a net positive source of MMHg this potentially suggests different reaction paths for MMHg generation below versus above the creek bed. Knowing the major sources and reaction pathways of MMHg generation in the creek is imperative for the development of an appropriate remediation plan.

This is the first study to use transient availability kinetics to predict MMHg production across seasons, light condition, and location. MMHg production is a complex process that is influenced by many factors, including the composition and activity of the methylating microbial community, the availability of Hg for methylation, and the rate of biotic and abiotic demethylation (Hsu-Kim 2013). Though there are surely more parameters that impact methylation and demethylation in EFPC periphyton, in our predictive models, light condition, season, and location explained over 80% of the variation in $k_{m,\ trans\ av}$ and $k_{d,\ trans\ av}$, indicating that these factors encompass the important drivers of MMHg production in EFPC. The ability to accurately predict MMHg production with these simple parameters has major implications for modeling MMHg risk. More research is needed to determine how well transient availability kinetics apply to periphyton in other ecosystems, and our research provides a good set of initial parameters with which to assess MMHg production in a wider set of ecosystems.

Our results also highlight the limitations of full availability kinetics in predicting MMHg production. No significant predictive models resulted when using light condition, location, and season as factors and rate potentials derived with full

availability kinetics. Additionally, transient availability rate potentials were correlated with ambient MMHg concentrations in EFPC periphyton whereas the full availability methylation rate potentials did not strongly correlate. These results indicate that the transient availability model is a more accurate predictor of MMHg ecosystem dynamics than the full availability model. If these results are shown to hold across ecosystems, predictive modeling combined with the transient availability kinetic model will be a powerful tool in predicting MMHg risk.

Methylation and demethylation rates are the product of the rate potential and the ambient concentration of Hg or MMHg. At the ambient Hg and MMHg concentrations present in EFPC, even small differences in the rate potential can dramatically change methylation and demethylation rates. Net MMHg calculated with our transient availability rate potentials (maximum of 41 ng/g-dw d in Downstream Light in the Summer) was much higher than net MMHg production estimates calculated with $k_{m,\ full\ av}$ and $k_{d,\ full\ av}$ (maximum of 5.2 ng/g-dw d in Downstream Light in the Fall). Estimates of net MMHg production differed by as much as 50 times between the calculation methods. This difference, in turn, substantially impacts estimates of MMHg flux in EFPC.

SUPPLEMENTAL DATA STATEMENT

The supplemental data section includes additional information on methods, QA/QC parameters for MMHg analysis, tables of calculated rate potentials, details on predictive models, and additional figures.

DATA ACCESSIBILITY STATEMENT

Data associated with this manuscript is available in the Supplementary Information file.

REFERENCES

Achá D, Hintelmann H, Yee J. 2011. Importance of sulfate reducing bacteria in mercury methylation and demethylation in periphyton from Bolivian Amazon region. Chemosphere. 82(6):911-916.

Achá D, Pabón CA, Hintelmann H. 2012. Mercury methylation and hydrogen sulfide production among unexpected strains isolated from periphyton of two macrophytes of the amazon. FEMS Microbiology Ecology. 80(3):637-645.

Arar EJ. 1997. Method 446.0: In vitro determination of chlorophylls a, b, c + c and pheopigments in marine and freshwater algae by visible spectrophotometry. United States Environmental Protection Agency: Washington, D.C. EPA/600/R-15/005.

Bancon-Montigny C, Yang L, Sturgeon RE, Colombini V, Mester Z. 2004. High-yield synthesis of milligram amounts of isotopically enriched methylmercury ($CH_3{}^{198}HgCl$). Applied Organometallic Chemistry. 18(2):57-64.

Battin TJ, Besemer K, Bengtsson MM, Romani AM, Packmann AI. 2016. The ecology and biogeochemistry of stream biofilms. Nature Reviews Microbiology. 14:251-263.

Black FJ, Poulin BA, Flegal AR. 2012. Factors controlling the abiotic photo-degradation of monomethylmercury in surface waters. Geochimica et Cosmochimica Acta. 84:492-507.

Bloom NS, Colman JA, Barber L. 1997. Artifact formation of methyl mercury during aqueous distillation and alternative techniques for the extraction of methyl mercury from environmental samples. Fresenius' Journal of Analytical Chemistry. 358(3):371-377.

Bravo AG, Bouchet S, Tolu J, Björn E, Mateos-Rivera A, Bertilsson S. 2017. Molecular composition of organic matter controls methylmercury formation in Boreal lakes. Nature Communications. 8:14255.

Brooks SC, Eller V, Dickson J, Earles J, Lowe K, Mehlhorn T, Olsen TA, DeRolph C, Watson D, Phillips D et al. 2017. Mercury content of sediments in east fork poplar creek: Current assessment and past trends. Oak Ridge National

Laboratory: Oak Ridge, TN. ORNL/TM-2016/578. OSTI ID: 1338545. DOI: 10.2172/1338545.

Brooks SC, Lowe K, Mehlhorn T, Olsen TA, Yin X, Fortner AM, Peterson M. 2018. Intraday water quality patterns in East Fork Poplar Creek with an emphasis on mercury and monomethylmercury. Oak Ridge National Laboratory: Oak Ridge, TN. ORNL/TM-2018/812. DOI: 10.2172/1437608.

Brooks SC, Southworth GR. 2011. History of mercury use and environmental contamination at the Oak Ridge Y-12 plant. Environmental Pollution. 159(1):219-228.

Christensen GA, Somenahally AC, Moberly JG, Miller CM, King AJ, Gilmour CC, Brown SD, Podar M, Brandt CC, Brooks SC et al. 2018. Carbon amendments alter microbial community structure and net mercury methylation potential in sediments. Applied and Environmental Microbiology. 84(3):e01049-01017.

Clarkson TW, Magos L, Myers GJ. 2003. The toxicology of mercury — current exposures and clinical manifestations. New England Journal of Medicine. 349(18):1731-1737.

Cleckner LB, Gilmour CC, Hurley JP, Krabbenhoft DP. 1999. Mercury methylation in periphyton of the Florida Everglades. Limnology and Oceanography. 44(7):1815-1825.

Desrosiers M, Planas D, Mucci A. 2006. Mercury methylation in the epilithon of Boreal shield aquatic ecosystems. Environmental Science & Technology. 40(5):1540-1546.

Dranguet P, Le Faucheur S, Slaveykova VI. 2017a. Mercury bioavailability, transformations, and effects on freshwater biofilms. Environmental Toxicology and Chemistry. 36(12):3194-3205.

Dranguet P, Slaveykova VI, Le Faucheur S. 2017b. Kinetics of mercury accumulation by freshwater biofilms. Environmental Chemistry. 14(7):458-467.

Gentès S, Taupiac J, Colin Y, André J-M, Guyoneaud R. 2017. Bacterial periphytic communities related to mercury methylation within aquatic plant roots from a temperate freshwater lake (south-western France). Environmental Science and Pollution Research. 24(23):19223-19233.

Gilmour C, Bell JT, Soren AB, Riedel G, Riedel G, Kopec AD, Bodaly RA. 2018. Distribution and biogeochemical controls on net methylmercury production in Penobscot River marshes and sediment. Science of The Total Environment. 640-641:555-569.

Gilmour CC, Podar M, Bullock AL, Graham AM, Brown SD, Somenahally AC, Johs A, Hurt RA, Bailey KL, Elias DA. 2013. Mercury methylation by novel microorganisms from new environments. Environmental Science & Technology. 47(20):11810-11820.

Graham AM, Aiken GR, Gilmour CC. 2012. Dissolved organic matter enhances microbial mercury methylation under sulfidic conditions. Environmental Science & Technology. 46(5):2715-2723.

Graham AM, Aiken GR, Gilmour CC. 2013. Effect of dissolved organic matter source and character on microbial hg methylation in Hg–S–DOM solutions. Environmental Science & Technology. 47(11):5746-5754.

Graham EB, Gabor RS, Schooler S, McKnight DM, Nemergut DR, Knelman JE. 2018. Oligotrophic wetland sediments susceptible to shifts in microbiomes and mercury cycling with dissolved organic matter addition. PeerJ. 6:e4575.

Grégoire DS, Poulain AJ. 2014. A little bit of light goes a long way: The role of phototrophs on mercury cycling. Metallomics. 6(3):396-407.

Hamelin S, Amyot M, Barkay T, Wang Y, Planas D. 2011. Methanogens: Principal methylators of mercury in lake periphyton. Environmental Science & Technology. 45(18):7693-7700.

Hsu-Kim H, Kucharzyk KH, Zhang T, Deshusses MA. 2013. Mechanisms regulating mercury bioavailability for methylating microorganisms in the aquatic environment: A critical review. Environmental Science & Technology. 47(6):2441-2456.

Huguet L, Castelle S, Schäfer J, Blanc G, Maury-Brachet R, Reynouard C, Jorand F. 2010. Mercury methylation rates of biofilm and plankton microorganisms from a hydroelectric reservoir in French Guiana. Science of The Total Environment. 408(6):1338-1348.

Jørgensen BB, Revsbech NP, Blackburn TH, Cohen Y. 1979. Diurnal cycle of oxygen and sulfide microgradients and microbial photosynthesis in a cyanobacterial mat sediment. Applied and Environmental Microbiology. 38(1):46.

Kis M, Sipka G, Maróti P. 2017. Stoichiometry and kinetics of mercury uptake by photosynthetic bacteria. Photosynthesis Research. 132(2):197-209.

Kucharzyk KH, Deshusses MA, Porter KA, Hsu-Kim H. 2015. Relative contributions of mercury bioavailability and microbial growth rate on net methylmercury production by anaerobic mixed cultures. Environmental Science: Processes & Impacts. 17(9):1568-1577.

Leclerc M, Planas D, Amyot M. 2015. Relationship between extracellular low-molecular-weight thiols and mercury species in natural lake periphytic biofilms. Environmental Science & Technology. 49(13):7709-7716.

Lehmann K, Singer A, Bowes MJ, Ings NL, Field D, Bell T. 2015. 16S rRNA assessment of the influence of shading on early-successional biofilms in experimental streams. FEMS Microbiology Ecology. 91(12):fiv129-fiv129.

Mangal V, Phung T, Nguyen TQ, Guéguen C. 2019a. Molecular characterization of mercury binding ligands released by freshwater algae grown at three photoperiods. Frontiers in Environmental Science. 6(155).

Mangal V, Stenzler BR, Poulain AJ, Guéguen C. 2019b. Aerobic and anaerobic bacterial mercury uptake is driven by algal organic matter composition and molecular weight. Environmental Science & Technology. 53(1):157-165.

Mauro J, Guimarães J, Hintelmann H, Watras C, Haack E, Coelho-Souza S. 2002. Mercury methylation in macrophytes, periphyton, and water – comparative studies with stable and radio-mercury additions. Analytical and Bioanalytical Chemistry. 374(6):983-989.

Meija J, Yang L, Caruso JA, Mester Z. 2006. Calculations of double spike isotope dilution results revisited. Journal of Analytical Atomic Spectrometry. 21(11):1294-1297.

Olsen TA, Brandt CC, Brooks SC. 2016. Periphyton biofilms influence net methylmercury production in an industrially contaminated system. Environmental Science & Technology. 50(20):10843-10850.

Olsen TA, Muller KA, Painter SL, Brooks SC. 2018. Kinetics of methylmercury production revisited. Environmental Science & Technology. 52(4):2063-2070.

Podar M, Gilmour CC, Brandt CC, Soren A, Brown SD, Crable BR, Palumbo AV, Somenahally AC, Elias DA. 2015. Global prevalence and distribution of genes and microorganisms involved in mercury methylation. Science Advances. 1(9):e1500675.

Revsbech NP, Jorgensen BB, Blackburn TH, Cohen Y. 1983. Microelectrode studies of the photosynthesis and O_2, H_2S, and pH profiles of a microbial mat1. Limnology and Oceanography. 28(6):1062-1074.

Riscassi A, Miller C, Brooks S. 2016. Seasonal and flow-driven dynamics of particulate and dissolved mercury and methylmercury in a stream impacted by an industrial mercury source. Environmental Toxicology and Chemistry. 35(6):1386-1400.

SAS Institute. 2018. JMP. 14 ed.: SAS Institute.

Schaefer JK, Morel FMM. 2009. High methylation rates of mercury bound to cysteine by geobacter sulfurreducens. Nature Geoscience. 2:123-126.

Schaefer JK, Rocks SS, Zheng W, Liang L, Gu B, Morel FMM. 2011. Active transport, substrate specificity, and methylation of Hg(II) in anaerobic bacteria. Proceedings of the National Academy of Sciences. 108(21):8714-8719.

US EPA. 2001a. US EPA method 1630: Methyl mercury in water by distillation aqueous ethylation, 523 purge, and trap,and cold vapor atomic fluorescence spectroscopy. U.S. EPA: Washington, D.C.

US EPA. 2001b. US EPA method 1631, revision D: Mercury in water by oxidation, purge, and trap, 526 and cold vapor atomic fluorescence spectroscopy. U.S. EPA: Washington, D.C.

Zhang J, Wang F, House JD, Page B. 2004. Thiols in wetland interstitial waters and their role in mercury and methylmercury speciation. Limnology and Oceanography. 49(6):2276-2286.

Zhao Y, Xiong X, Wu C, Xia Y, Li J, Wu Y. 2018. Influence of light and temperature on the development and denitrification potential of periphytic biofilms. Science of The Total Environment. 613-614:1430-1437.

Žižek S, Horvat M, Gibičar D, Fajon V, Toman MJ. 2007. Bioaccumulation of mercury in benthic communities of a river ecosystem affected by mercury mining. Science of The Total Environment. 377(2):407-415.

Table 1. Water Quality data from Upstream and Downstream sites at each seasonal experiment[a]

	Winter		Spring		Summer		Fall	
	Upstream	Downstream	Upstream	Downstream	Upstream	Downstream	Upstream	Downstream
Temp (C°)	10.2	9.39	16.1	15.2	19.3	21.3	11.5	9.56
pH	7.37	7.11	7.87	8.08	7.86	7.74	7.94	7.51

Cond (µS/cm)	405.9	239.6	355.0	302.0	364.6	324.4	331.9	305.9
DO (mg/L)	11.5	11.6	9.73	9.34	8.46	7.65	10.6	10.0
TSS (mg/L)	2.69	4.72	2.57	2.33	2.40	7.60	1.67	1.00
DOC (mg/L)	--	--	--	--	--	--	2.05	2.72
Filtered[b] MMHg (ng/L)	0.047	0.092	0.093	0.332	0.103	0.462	0.097	0.254
Unfiltered MMHg (ng/L)	0.062	0.121	0.137	0.421	0.136	0.699	0.094	0.267
Filtered[b] Total Hg (ng/L)	51.0	8.80	49.6	12.6	52.0	19.4	--	--
Unfiltered Total Hg (ng/L)	117	62.3	95.1	50.8	90.5	130	--	--

DO = dissolved oxygen, TSS = total suspended solids, DOC = dissolved organic carbon

[a]Due to legacy contamination, discharge from a wastewater treatment plant and nonpoint fertilizer runoff, EFPC is eutrophic with respect to N and P over the studied reach. Nitrate concentrations are above 8 mg L^{-1} and phosphate concentrations are above 0.1 mg L^{-1}.

[b]Filtered through 0.2 µm pore size polyethersulfone membrane filter

Figures

Figure 1. Ambient Hg (a), ambient MMHg (b), and Percent MMHg (c) in EFPC periphyton. Hg bars are the average of triplicate samples. Ambient MMHg in the periphyton was measured concomitantly with $MM^{201}Hg$ and $MM^{202}Hg$ in the methylation/demethylation assays (n = 15 per treatment) and normalized by the average dry weight of periphyton per disc measured in the wet/dry assay for each respective treatment. Error bars represent one standard error.

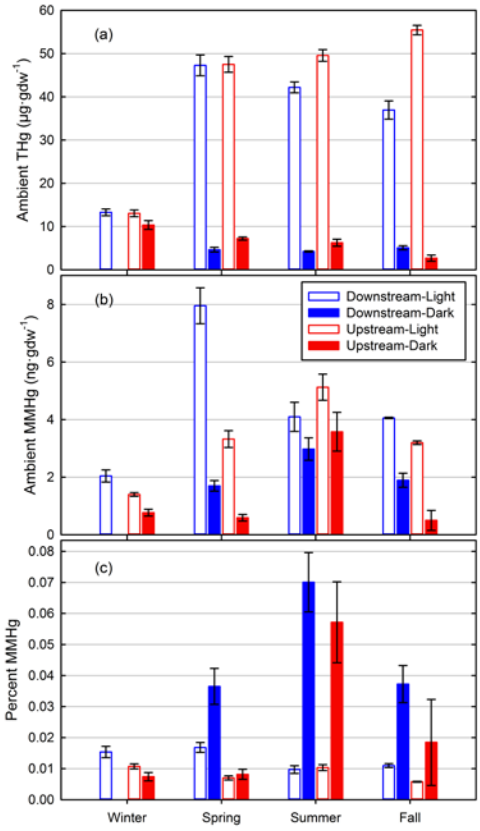

Figure 2. (a) Transient availability model methylation rate potentials ($k_{m,\ trans\ av}$, d^{-1}) in periphyton. Bars represent the average of triplicate samples. Error bars represent one standard error; (b) Predictive modelling output for methylation, $k_{m,\ trans\ av}$ = Season + Light; $k_{m,\ trans\ av}$ is the methylation rate potential (d^{-1}) determined from the transient availability model. Predictive equation: $k_{m,\ trans\ av} = 6.51 \times 10^{-4} + 1.42 \times 10^{-5}\text{Fall} - 1.27 \times 10^{-4}\text{Spring} + 4.44 \times 10^{-4}\text{Summer} - 3.31 \times 10^{-4}\text{Winter} + 2.13 \times 10^{-4}\text{Light} - 2.13 \times 10^{-4}\text{Dark}$.

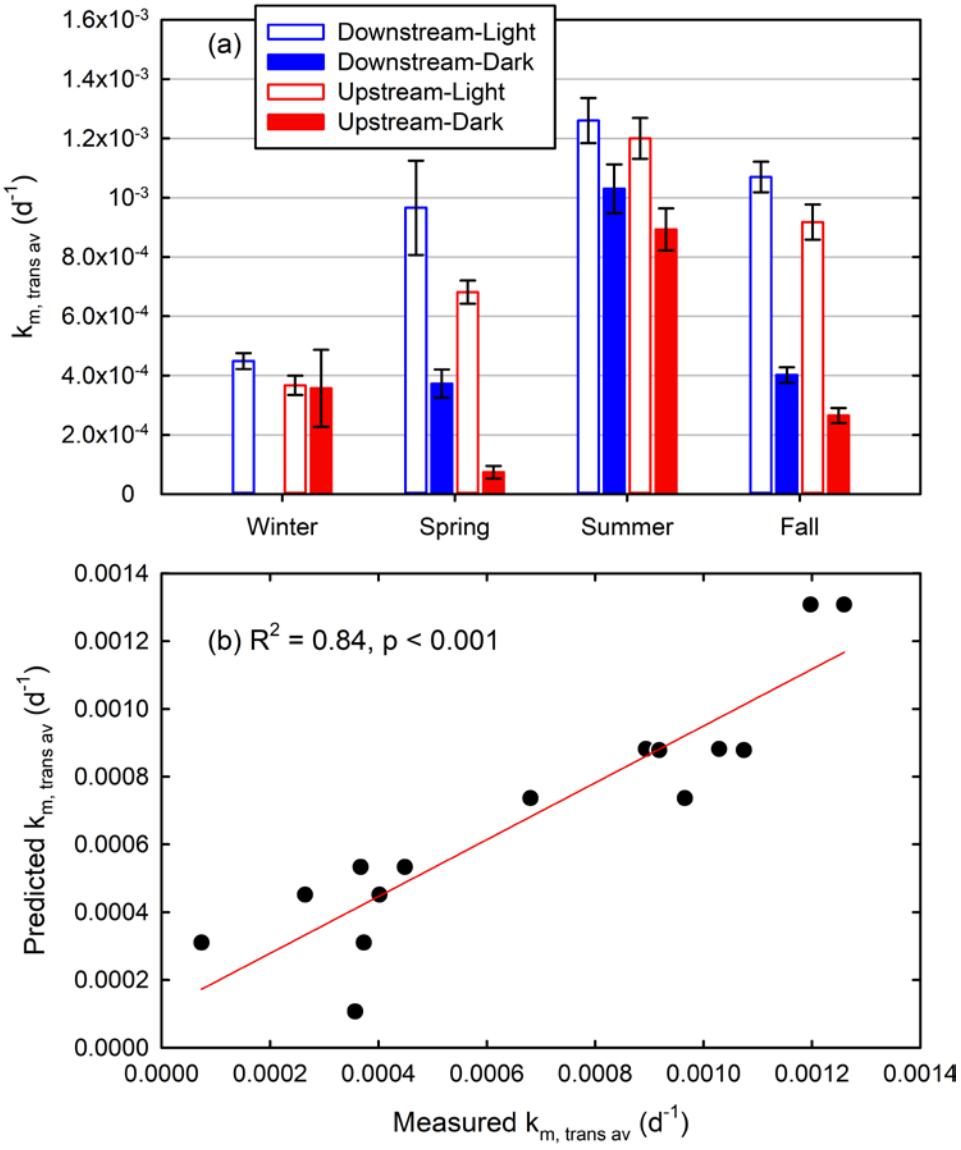

Figure 3. (a) Demethylation rate potentials ($k_{d,\ trans\ av}$, d^{-1}) in periphyton. Bars represent the average of triplicate samples. Error bars represent one standard error; (b) Predictive modeling output for demethylation, ln($k_{d,\ trans\ av}$) = Season + Light + Location. $k_{d,\ trans\ av}$ is the demethylation rate potential (d^{-1}) determined from the transient availability model. Predictive equation: ln($k_{d,\ trans\ av}$) = 1.22 - 0.477Fall + 0.657Spring + 0.359Summer – 0.538Winter – 0.309Downstream + 0.309Upstream + 0.784Dark – 0.784Light.

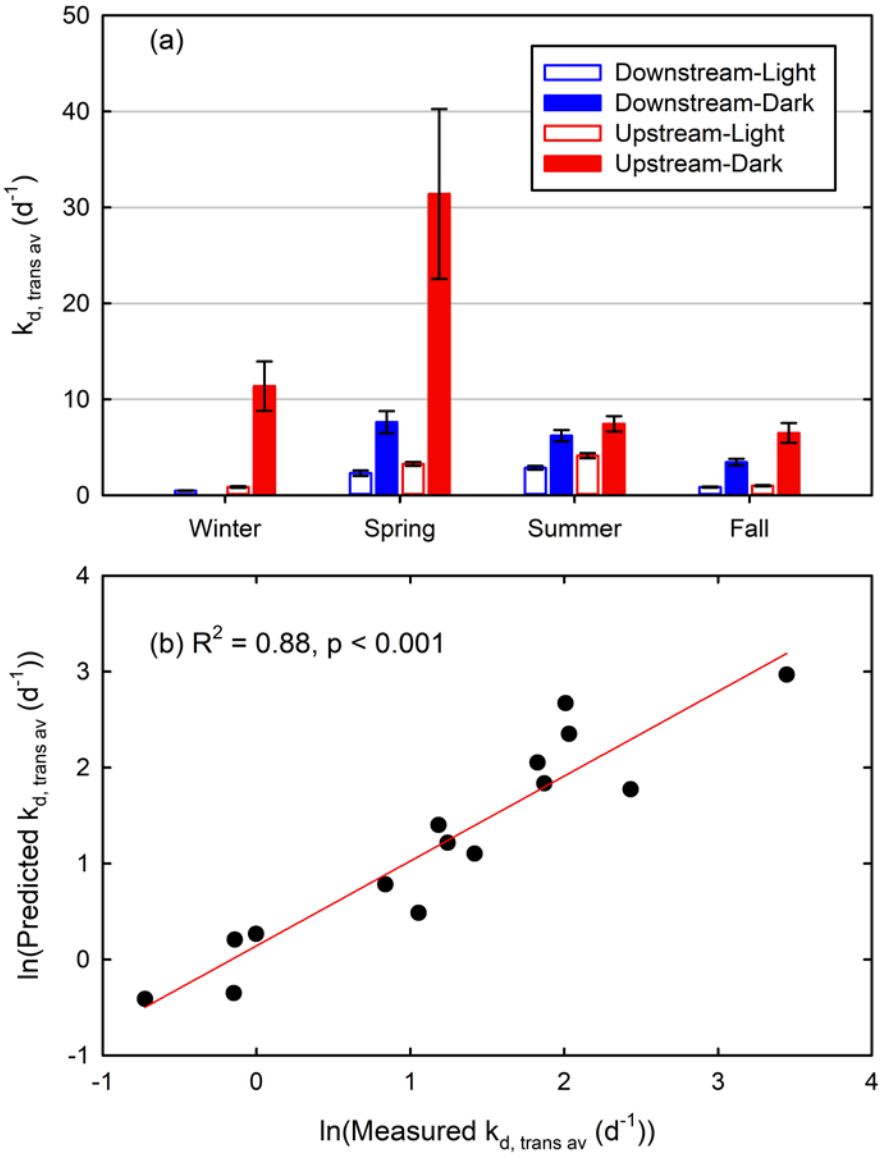

Figure 4. Net methylation (ng·gdw^{-1}·d^{-1}) in periphyton. Net methylation was calculated with equation 3, using $k_{m,\ trans\ av}$ and $k_{d,\ trans\ av}$ rate potentials multiplied by the average ambient Hg or MMHg in the periphyton. Bars represent the average of triplicate samples. Error bars represent one standard error.

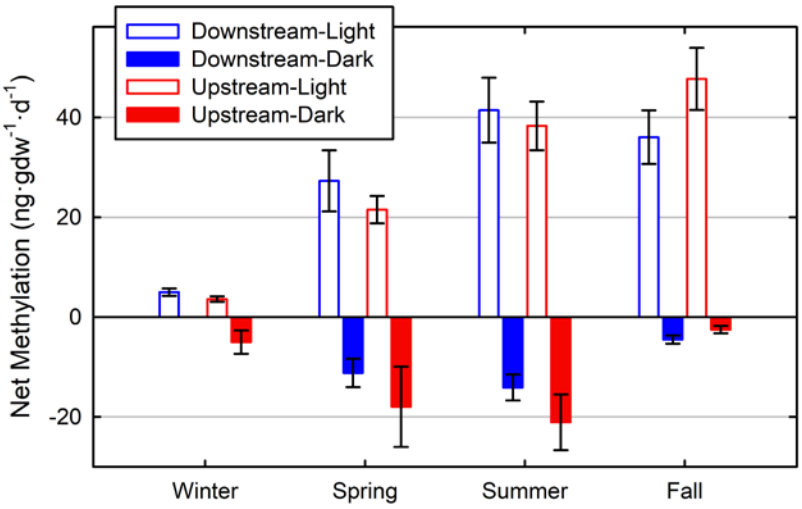

Figure 5. Ratio of Transient availability rate potentials to full availability rate potentials (calculated at 1d): (a) methylation; (b) demethylation. No data were available for methylation Spring Upstream Dark due to a zero value for $k_{m,\ full\ av}$ at that time point. Error bars represent one standard error.